International Journal of Thermophysics, Vol. 27, No. 5, September 2006 (© 2006)
DOI: 10.1007/s10765-006-0130-6

Natural Convection along a Vertical Thin Cylinder with Uniform and Constant Wall Heat Flux

F. Gori,[1,2] M. G. Serranò,[1] and Y. Wang[1]

Received March 18, 2006

A theoretical investigation is carried out to study natural convection around a vertical thin cylinder, or a needle, heated at uniform and constant wall heat flux in order to compare the analytical solutions of the present work with previous experimental results. The local non-similarity solution with the first level of truncation, proposed by Minkowycz and Sparrow, is used. The temperature and velocity distributions are calculated for fluids with several Prandtl numbers. The analytical solutions of this work are compared to experimental results carried out with needles of diameters ranging from 0.6 to 1.5 mm and fluids with Prandtl numbers in the range Pr = 0.7–730. The agreement is reasonable good.

KEY WORDS: local non-similarity solution; natural convection; uniform heat flux; vertical thin cylinder.

1. INTRODUCTION

Several papers have been published on natural convection around vertical isothermal cylinders. Elenbaas [1] employed the Langmuir stagnant film model, and the natural convection problem was simplified as a heat conduction one. Also employing the stagnant film model, Sparrow and Gregg [2],[3] solved this problem by a series expansion. Minkowycz and Sparrow [4] studied the natural convection along a vertical cylinder with a constant surface temperature by a local non-similarity solution. Kuiken [5] and Fujii and Uehara [6] studied the heat transfer of non-isothermal vertical cylinders with large curvatures by series solutions.

[1]Department of Mechanical Engineering, University of Rome "Tor Vergata," Via del Politecnico 1, 00133 Rome, Italy.
[2]To whom correspondence should be addressed. E-mail: gori@uniroma2.it

The aim of the present paper is to study analytically the problem of natural convection along a vertical needle with uniform and constant wall heat flux, which is the thermal boundary condition used in previous experiments. Experimental measurements of the thermal conductivity of fluids and porous media have been carried out with thermal probes, consisting of needles with diameters ranging from 0.6 to 1.5 mm, heated at a uniform and constant wall heat flux [7]–[15]. Comparisons of the analytical solutions of this work with the experimental results of Refs. 9 and 15 are carried out.

2. ANALYSIS

A vertical needle, immersed in a fluid, is heated at a uniform and constant wall heat flux, q_w. The fluid properties are assumed as constant except for the density, which is considered variable only to the extent it contributes to the buoyancy forces.

Under steady-state conditions, the governing equations of this problem, in cylindrical co-ordinates, are similar to those studied by Minkowycz and Sparrow [4]:

$$\frac{\partial (ru)}{\partial x} + \frac{\partial (rw)}{\partial r} = 0 \tag{1}$$

$$u\frac{\partial u}{\partial x} + w\frac{\partial u}{\partial r} = g\beta (T - T_\infty) + \frac{\nu}{r}\frac{\partial}{\partial r}\left(r\frac{\partial u}{\partial r}\right) \tag{2}$$

$$u\frac{\partial T}{\partial x} + w\frac{\partial T}{\partial r} = \frac{\alpha}{r}\frac{\partial}{\partial r}\left(r\frac{\partial T}{\partial r}\right) \tag{3}$$

where u and w are the velocity components, respectively, in axial and radial directions, and T is the temperature. The boundary conditions are

$$u(x,r) = w(x,r) = \frac{\partial T(x,r)}{\partial r} + \frac{q_w}{k} = 0 \quad \text{at } r = r_0 \tag{4}$$

$$u(x,r) = w(x,r) = T(x,r) - T_\infty = 0 \quad \text{at } r \to \infty \tag{5}$$

For the local non-similarity solution, two new co-ordinates η and ξ are introduced;

$$\eta = \frac{(Gr_0^*)^{1/4}}{2\sqrt{2}} \frac{(r/r_0)^2 - 1}{(x/r_0)^{1/4}} \tag{6}$$

$$\xi = \frac{2\sqrt{2}(x/r_0)^{1/4}}{(Gr_0^*)^{1/4}}. \tag{7}$$

The stream function is defined as

$$\psi = 2\sqrt{2}\nu r_0^{1/4}(Gr_0^*)^{1/4}x^{3/4}f(\xi,\eta) \tag{8}$$

where f is the dimensionless stream function. The dimensionless temperature is defined as

$$\theta = \frac{T - T_\infty}{q_w r_0/k}. \tag{9}$$

The velocity components are obtained from

$$u = \frac{1}{r}\frac{\partial\psi}{\partial r}, \quad w = -\frac{1}{r}\frac{\partial\psi}{\partial x}. \tag{10}$$

Equations (1)–(3) can be rewritten, in terms of the new variables as

$$\frac{\partial}{\partial\eta}\left[(1+\xi\eta)\frac{\partial^2 f}{\partial\eta^2}\right] + 3f\frac{\partial^2 f}{\partial\eta^2} - 2\left(\frac{\partial f}{\partial\eta}\right)^2 + \theta = \xi\left[\frac{\partial f}{\partial\eta}\frac{\partial^2 f}{\partial\eta\partial\xi} - \frac{\partial^2 f}{\partial\eta^2}\frac{\partial f}{\partial\xi}\right] \tag{11}$$

$$\frac{1}{Pr}\frac{\partial}{\partial\eta}\left[(1+\xi\eta)\frac{\partial\theta}{\partial\eta}\right] + 3f\frac{\partial\theta}{\partial\eta} = \xi\left[\frac{\partial f}{\partial\eta}\frac{\partial\theta}{\partial\xi} - \frac{\partial\theta}{\partial\eta}\frac{\partial f}{\partial\xi}\right]. \tag{12}$$

As a first approximation, the terms with the partial derivatives, with respect to ξ, on the right-hand side of Eqs. (11) and (12) are neglected. Rearranging the terms on the left-hand side of Eqs. (11) and (12), the local non-similarity equations with the first level of truncation [4], can be obtained as follows:

$$\frac{\partial^3 f}{\partial\eta^3} + \left(\frac{3f+\xi}{1+\xi\eta}\right)\frac{\partial^2 f}{\partial\eta^2} = \frac{2\left(\frac{\partial f}{\partial\eta}\right)^2 - \theta}{1+\xi\eta} \tag{13}$$

$$\frac{\partial^2\theta}{\partial\eta^2} + \left(\frac{3Prf+\xi}{1+\xi\eta}\right)\frac{\partial\theta}{\partial\eta} = 0 \tag{14}$$

The boundary conditions, Eqs. (4) and (5), become, in dimensionless form:

$$f(\xi,\eta) = f'(\xi,\eta) = 0, \quad \theta'(\xi,\eta) + \frac{1}{2}\xi = 0 \quad \text{at } \eta = 0; \tag{15}$$

$$f'(\xi,\eta) = \theta(\xi,\eta) = 0 \quad \text{at } \eta = \infty. \tag{16}$$

The local non-similarity solution of the higher level of truncation has higher precision but the solution of the first level of truncation is accurate enough that the difference between the solution of the first and third levels of truncation, according to Ref. 4, is negligible for natural convection over a cylinder. The conclusions of Ref. 4 can also be applied to the present analytical solutions because the main difference is due to the thermal boundary conditions.

3. RESULTS AND DISCUSSION

The numerical method suggested in Ref. 4 was employed to solve Eqs. (13)–(16). The velocity and temperature distributions have been obtained for fluids with various Prandtl numbers. For each fluid the maximum f', or $f'_{\max}$, increases as ξ increases. When η reaches a certain value, f' attains its maximum value and then decreases gradually with a continuous increase of η. Finally, f' approaches zero as $\eta \to \infty$. The maximum f', or $f'_{\max}$, is higher for a smaller Prandtl number. The corresponding critical η, η_c, changes with ξ. Although the location of the maximum f', or $f'_{\max}$, increases with ξ for natural convection, the location of $f'_{\max}$, η_c, appears to be a weak function of ξ, as found in Ref. 4 for a constant surface temperature.

The dimensionless temperatures for different value of ξ and Prandtl numbers, indicate that, for a fixed ξ, θ decreases sharply when η is smaller. With increasing η, the rate of decrease of θ becomes smaller. As η is approaching infinity, θ approaches zero. For a fixed Pr and η, θ increases with ξ. The dimensionless temperature on the needle surface, θ_0, is reported in Fig. 1 for Pr = 0.708, 7.02, and 50, i.e., for air, water, and oil. Figure 1 shows that θ_0 increases with ξ and decreases with Pr. Similar conclusions can be drawn for Pr = 2.5 and 10, as reported in Fig. 2.

The heat transfer coefficient and the local Nusselt number can be determined from the following relations:

$$h = \frac{k}{r_0 \theta(\xi, 0)} \tag{17}$$

$$\frac{Nu}{Gr_0^*} = \frac{\xi^4}{64\theta(\xi, 0)}. \tag{18}$$

The mean Nusselt number can be obtained by

$$\frac{Nu_m}{Gr_0^*} = \frac{1}{16} \int_0^{\xi} \frac{\xi^3 d\xi}{\theta(\xi, 0)} \tag{19}$$

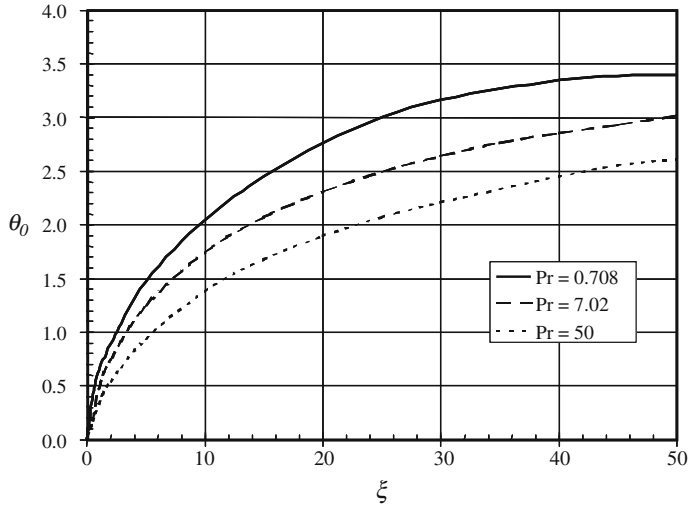

Fig. 1. Dimensionless temperature on the needle surface for air, water, and oil.

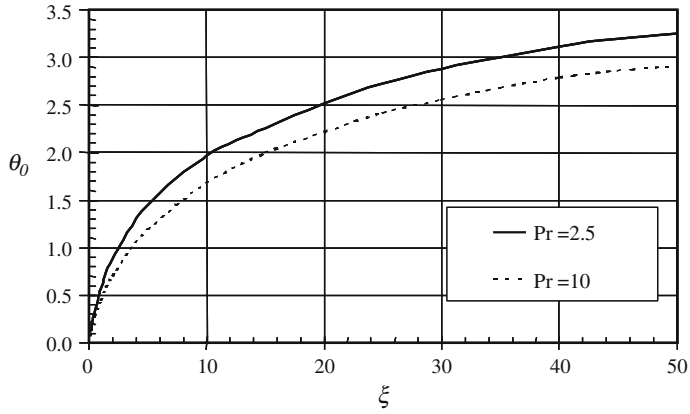

Fig. 2. Dimensionless temperature on the needle surface for water at two temperatures.

Since θ (ξ,0) is a function of ξ only, both Nu/Gr_0^* and Nu_m/Gr_0^* are also functions of ξ. The local Nu and mean Nu_m Nusselt numbers, reported vs. ξ in Figs. 3 and 4, respectively, show that both increase as ξ increases. The ratio Nu_m/Nu is equal to 2 at ξ = 0.01, but it decreases with increasing ξ for the three fluids (Pr = 0.708, Pr = 7.02, Pr = 50). For ξ = 2 the ratio

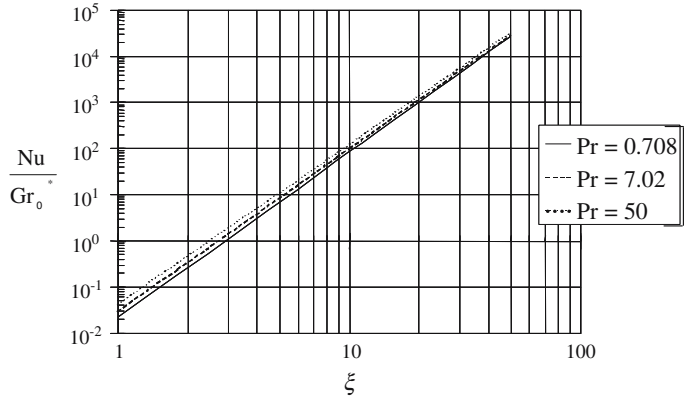

Fig. 3. Local Nusselt number for air, water, and oil.

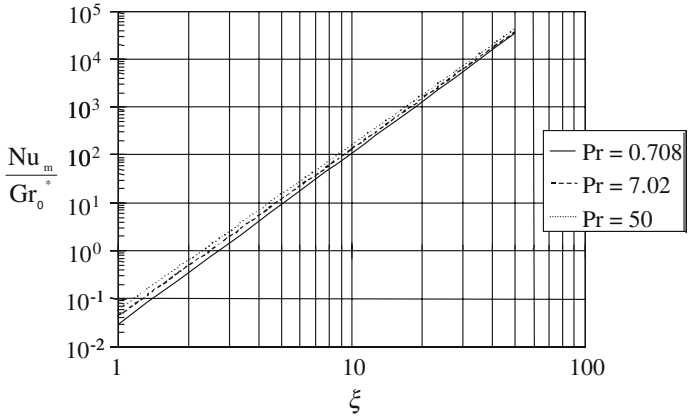

Fig. 4. Mean Nusselt number for air, water, and oil.

Nu_m/Nu is equal to 1.29 for air (Pr = 0.708), 1.35 for water (Pr = 7.02), and 1.35 for oil (Pr = 50).

The analytical predictions of this work are compared to the experimental data measured in water, [9], with the Prandtl number variable in the range from 2.5 to 10. The experimental data of Ref. 9, obtained with a maximum uncertainty of $\pm 15\%$, and the analytical results of the present work are reported in Table I and Fig. 5.

The analytical results of the present work for Pr = 2.5, continuous line, are not reported between $\xi = 50$ and 60 because they are coincident with those obtained for Pr = 10 (dotted line). The comparison shows that

Table I. Comparisons among the Analytical Results of this Work and the Experimental Data of Gori et al. [9]

	Experimental data of Gori et al. [9]			This work	
Pr	Nu	Gr_0^*	Nu/Gr_0^*	Nu/Gr_0^*	Deviation
10.49	97.2	2.3×10^{-4}	$4.2\times10^{+5}$	$4.5\times10^{+5}$	7%
10.03	102.1	3.4×10^{-4}	$3.0\times10^{+5}$	$3.0\times10^{+5}$	−1%
9.50	108.4	5.0×10^{-4}	$2.2\times10^{+5}$	$2.2\times10^{+5}$	1%
9.24	113.0	5.9×10^{-4}	$1.9\times10^{+5}$	$1.7\times10^{+5}$	−11%
9.21	93.5	1.2×10^{-3}	$7.7\times10^{+4}$	$8.5\times10^{+4}$	10%
8.93	98.5	1.7×10^{-3}	$5.7\times10^{+4}$	$5.7\times10^{+4}$	0%
8.82	102.1	1.9×10^{-3}	$5.5\times10^{+4}$	$5.5\times10^{+4}$	0%
8.65	113.5	8.2×10^{-4}	$1.4\times10^{+5}$	$1.2\times10^{+5}$	−14%
6.69	92.1	4.4×10^{-3}	$2.1\times10^{+4}$	$2.3\times10^{+4}$	11%
6.03	89.3	4.8×10^{-3}	$1.9\times10^{+4}$	$2.1\times10^{+4}$	14%
6.01	90.5	4.8×10^{-3}	$1.9\times10^{+4}$	$2.1\times10^{+4}$	15%
3.98	108.9	1.9×10^{-2}	$5.7\times10^{+3}$	$5.6\times10^{+3}$	−1%
3.91	110.7	1.3×10^{-2}	$8.4\times10^{+3}$	$8.0\times10^{+3}$	−5%
3.69	115.9	2.3×10^{-2}	$5.0\times10^{+3}$	$4.7\times10^{+3}$	−7%
3.61	113.8	2.4×10^{-2}	$4.7\times10^{+3}$	$4.4\times10^{+3}$	−5%
3.55	117.9	2.6×10^{-2}	$4.6\times10^{+3}$	$4.2\times10^{+3}$	−8%
3.47	120.0	2.7×10^{-2}	$4.4\times10^{+3}$	$4.0\times10^{+3}$	−9%
3.41	114.8	2.8×10^{-2}	$4.1\times10^{+3}$	$3.9\times10^{+3}$	−5%
2.64	116.4	5.4×10^{-2}	$2.2\times10^{+3}$	$2.1\times10^{+3}$	−3%
2.59	115.9	5.7×10^{-2}	$2.0\times10^{+3}$	$2.1\times10+^{3}$	2%
2.53	111.7	6.0×10^{-2}	$1.9\times10^{+3}$	$1.9\times10^{+3}$	1%

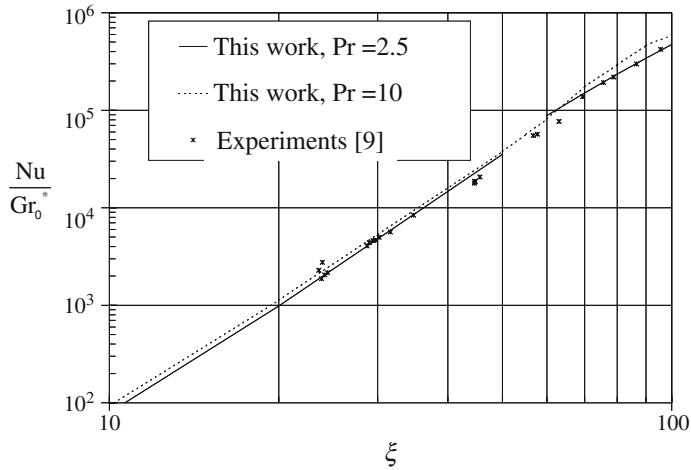

Fig. 5. Comparison with the experimental data of Gori et al. [9].

Table II. Comparisons among the Analytical Results of This Work, Experimental data of Gori and Coppa [15], and Eq. (20)

			Nu	*Nu*	*Nu*	
Fluid	*Pr*	Gr_0^*	Experiments Gori and Coppa [15]	Eq. (20)	This work	Deviation
Air	0.7	2.28×10^{-3}	62.5	59.3	62.7	0.3%
Dibutyl phthalate	730	2.96×10^{-5}	77.4	69.1	77.3	−0.1%
Ethylene glycol	186	2.94×10^{-4}	68.2	74.3	76.2	11.7%
Silicon oil	71.8	1.06×10^{-2}	86.4	92.8	96.7	11.9%

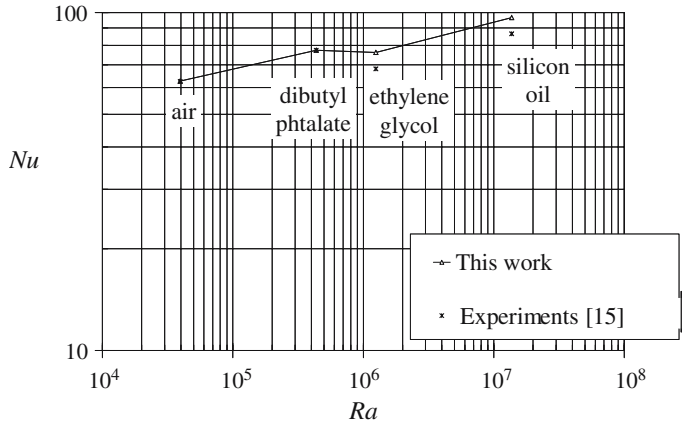

Fig. 6. Comparison with the experimental data of Gori and Coppa [15].

the experimental data are predicted with an average deviation of 6.7% and a maximum deviation of 15%, i.e., within the experimental uncertainty.

The present analytical approach has been used to predict the experimental data of Ref. 15, reported in Table II and Fig. 6. The experiments have been performed with air, dibutyl phthalate, ethylene glycol, and silicon oil with an overall uncertainty of ±1–2%. The Rayleigh numbers are 3.9×10^4 for air, 4.3×10^5 for dibutyl phthalate, 1.3×10^6 for ethylene glycol, and 1.4×10^7 for silicon oil. Figure 6 presents the analytical solutions of this work, which appear in agreement with the experiments, with a maximum deviation of 11.8%. The percent difference is also reported in Table II.

The analytical results of the present work are also compared to the data predicted by the following empirical relation, modified on the basis

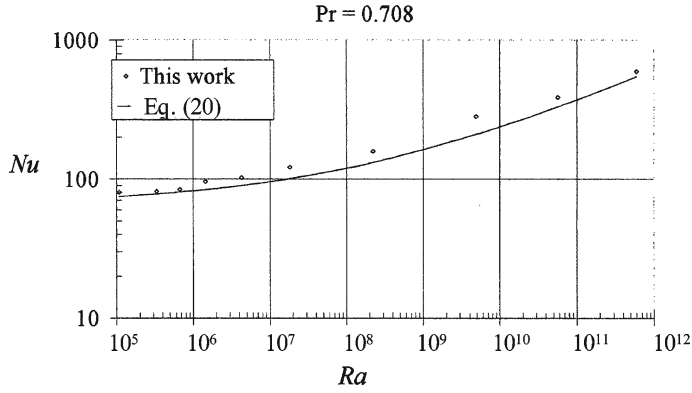

Fig. 7. Comparison with Eq. (20) for air.

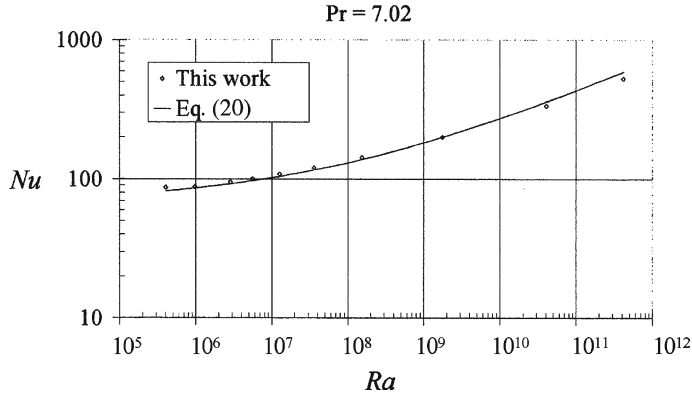

Fig. 8. Comparison with Eq. (20) for water.

of the expression of Ref. 16:

$$Nu = \frac{4}{3}\left[\frac{7Gr_0{}^*Pr^2}{5\,(20+21Pr)}\right]^{1/4} + \left[\frac{4\,(272+315Pr)}{35\,(64+63Pr)}\right]\frac{L}{D} \tag{20}$$

for the Prandtl numbers of 0.708, 7.02, and 50. Comparisons with air, reported in Fig. 7, show a maximum difference of 25% at $Ra = 5\times10^9$. Comparisons with water, reported in Fig. 8, show a maximum difference of 12%, while comparisons with oil, reported in Fig. 9, show a maximum difference of 16% for $Ra = 2\times10^{12}$.

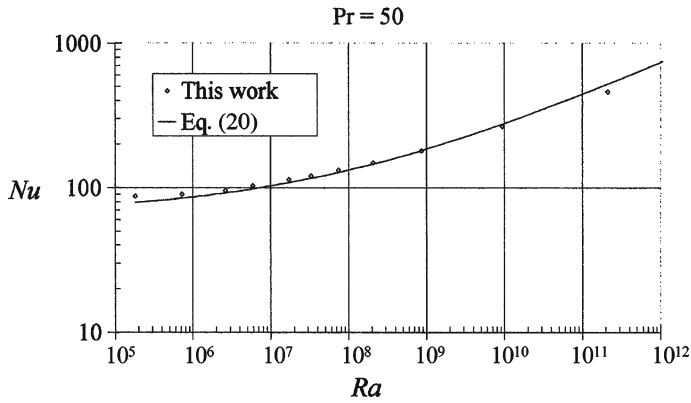

Fig. 9. Comparison with Eq. (20) for oil.

4. CONCLUSIONS

The local non-similarity solution with the first level of truncation is employed in this work to study natural convection around a needle with uniform and constant wall heat flux. The temperature distribution and the velocity profile are obtained in a wide range of Prandtl numbers. The present analytical solutions are compared to experimental results, obtained with needles used to measure the thermal conductivity of fluids. The analytical results of this work are in good agreement with the experimental data and with an empirical expression correlating previous experimental data from the literature.

ACKNOWLEDGMENTS

The authors thank ASI (Agenzia Spaziale Italiana) for partial support. The authors thank Dr. G. Foschi for help given during the preparation of the manuscript.

NOMENCLATURE

Symbols

D	Diameter of the needle (m)
f	Dimensionless stream function
$f' = \frac{\partial f}{\partial \eta}$	
g	Acceleration of gravity ($m \cdot s^{-2}$)
$Gr_0^* = g\beta q_w r_0^4/(k\nu)$	Modified Grashof number
h	Heat transfer coefficient ($W \cdot m^{-2} \cdot K^{-1}$)

h_m	Mean heat transfer coefficient ($W \cdot m^{-2} \cdot K^{-1}$)
k	Thermal conductivity ($W \cdot m^{-1} \cdot K^{-1}$)
L	Needle length (m)
$Nu = h\ x\ /\ k$	Nusselt number
$Nu_m = h_m x / k$	mean Nusselt number
$Pr = \nu\ /\ \alpha$	Prandtl number
q_w	Wall heat flux ($W \cdot m^{-2}$)
r	Radial coordinate (m)
$Ra = Gr_0^* Pr$	Rayleigh number
r_0	Needle radius (m)
T	Temperature (K)
T_∞	Stagnant temperature (K)
u	Axial velocity ($m \cdot s^{-1}$)
w	Radial velocity ($m \cdot s^{-1}$)
x	Axial coordinate (m)

Greek Symbols

α	Thermal diffusivity ($m^2 \cdot s^{-1}$)
β	Coefficient of thermal expansion (K^{-1})
η	Pseudo-similarity variable, Eq. (6)
ν	Kinematics viscosity ($m \cdot s^{-1}$)
θ	Dimensionless temperature, Eq. (9)
$\theta' = \frac{\partial \theta}{\partial \eta}$	
θ_0	Dimensionless wall temperature
ρ	Density ($kg \cdot m^{-3}$)
ξ	Stretched x coordinate, Eq. (7)
ψ	Stream function, Eq. (8), ($m^3 \cdot s^{-1}$)

Subscript

c	Critical
m	Mean
max	Maximum

REFERENCES

1. W. Elenbaas, *J. Appl. Phys.* **19**:1148 (1948).
2. E. M. Sparrow and J. L. Gregg, *Trans. ASME* 435 (1956).
3. E. M. Sparrow and J. L. Gregg, *Trans. ASME* 1823 (1956).
4. W. J. Minkowycz and E. M. Sparrow, *Trans. ASME*, *J. Heat Transfer* **96**:178 (1974).
5. H. K. Kuiken, *Int. J. Heat Mass Transfer* **11**:1141 (1968).
6. T. Fujii and H. Uehara, *Int. J. Heat Mass Transfer* **13**:607 (1970).
7. F. Gori and M. Pietrafesa, in *Fundamental Experimental Measurements in Heat Transfer*, ASME-WAM, Paper HT-7A-5, HTD Vol. 179, D. E. Beasley and J. L. S. Chen, eds., Book N. H00663–1991, Atlanta (1991), pp. 83–98.

8. F. Gori and M. Pietrafesa, *Proc. 10th Int. Heat Transfer Conf.*, Vol. 5, Brighton, United Kingdom (1994), pp. 349–354.
9. F. Gori, P. Coppa, and M. Pietrafesa, *Adv. Eng. Heat Transfer, Proc. Second Baltic Heat Transfer Conf.*, Southampton (1995), pp. 101–111.
10. F. Gori, C. Marino, and M. Pietrafesa, *Int. Commun. Heat Mass Transfer* **28**:1091 (2001).
11. F. Gori and S. Corasaniti, *5th World Conf. Exptal. Heat Transfer, Fluid Mechanics and Thermodyn.*, Vol. 2 (2001), pp. 1257–1262.
12. F. Gori and S. Corasaniti, *HTD-24152, Int. Mech. Eng. Cong. Expo. (IMECE)*, ASME (2001), pp. 1–8.
13. F. Gori and S. Corasaniti, *Microgravity and Space Station Utilization* **2**:23 (2001).
14. F. Gori and S. Corasaniti, *J. Heat Transfer* **126**:1001 (2002).
15. F. Gori and P. Coppa, *Proc. ESDA 2002*:6th *Biennial Conf. Eng. Systems Design Anal.*, Instanbul, Turkey, July 8–11 (2002).
16. E. J. Le Fevre and A. J. Ede, *Proc. IX Congress for Appl. Mech.*, Vol. 4, Brussels (1956), pp. 175–183.